# Low-energy photodetachment of $Ga^-$ and elastic electron scattering from neutral Ga

Kedong Wang*
*College of Physics and Materials Science, Henan Normal University, Xinxiang 453007, People's Republic of China*

Oleg Zatsarinny† and Klaus Bartschat‡
*Department of Physics and Astronomy, Drake University, Des Moines, Iowa 50311, USA*

(Received 20 June 2016; published 1 August 2016)

We present a comprehensive study of the photodetachment of the negative gallium ion and elastic electron scattering from neutral Ga for photon and electron energies ranging from threshold to 12 eV. The calculations are carried out with the $B$-spline $R$-matrix method. A multiconfiguration Hartree-Fock method with nonorthogonal term-dependent orbitals is employed to generate accurate initial- and final-state wave functions. The close-coupling expansions include the $4s^2 4pnl(kl)$ bound and continuum states of Ga and the $4s$-excited autoionizing states $4s4p^2$. The calculated photodetachment and elastic cross sections exhibit prominent resonance features. In order to clarify the origin of these resonances, the contributions of the major ionization channels to the partial cross sections are analyzed in detail.

DOI: 10.1103/PhysRevA.94.023402

## I. INTRODUCTION

Negative ions represent a special niche of atomic physics and offer excellent opportunities for studies of atomic structure, dynamics, and interactions in systems characterized by the binding of an extra electron to a neutral atom in a short-range potential. They are directly involved in the processes of radiation absorption in stellar (including solar) atmospheres, electronegative gas electric discharges and breakdown phenomena, and processes in the Earth's atmosphere [1]. Because of the diffuse character of the wave function and the weak binding of the outer electrons, negative ions provide an excellent test ground for theoretical and computational models dealing with highly correlated systems. Excited states of negative ions may appear as prominent features in photodetachment spectra, thereby revealing details of their structure and dynamics. Because of their unique properties, negative ions have been the target of numerous experimental and theoretical investigations.

Gallium is an important element for modern astrophysics [2] and plays a significant role in solving the problem of the generation of heavy elements in the universe. The stable negative ion of Ga has been studied both experimentally and theoretically with emphasis on the electron affinity. Arnau *et al.* [3] used a multireference single and double configuration-interaction (CI) method to obtain the electron affinity for $Ga^-$ as 0.29 eV. Wijesundera [4] carried out a multiconfiguration Dirac-Fock calculation and predicted an electron affinity of 0.305 eV. Eliav *et al.* [5] reported a value of 0.301 eV using the relativistic coupled-cluster method. Later, the electron affinity was established experimentally by laser photoelectron spectroscopy as $0.43 \pm 0.03$ eV [6]. While the fine-structure splitting was estimated as 0.072 eV, it was not resolved by the apparatus. Given that the statistical weighting factors for fine-structure levels are proportional to $(2J + 1)$, where $J$ is the total electronic angular momentum, the experimental result is likely close to the fine-structure-averaged value.

The experimental value differs considerably from all available theoretical predictions, thus indicating strong electron correlations in the ground state of $Ga^-$. In an attempt to resolve this discrepancy, Sundholm *et al.* [7] carried out an additional study by comparing electron affinities calculated at the numerical multiconfiguration Hartree-Fock level and at coupled-cluster levels using Gaussian basis sets. The electron affinity of 0.297(13) eV obtained in this work is still 0.133 eV smaller than the experimental value.

The only available experimental data for photodetachment of $Ga^-$ originate from the measurements by Feldmann *et al.* [8], who used a crossed-beam apparatus and reported the photodetachment cross sections for a set of negative ions including $Ga^-$. A rather high uncertainty in the absolute values, however, was estimated as about 50%.

To our knowledge, the only published study of the elastic cross section for electron scattering from Ga was performed by Felfli *et al.* [9] who used the complex angular-momentum approach. They predict a strong shape resonance that dominates the low-energy regime. In addition to investigating the photodetachment process in detail, our goal is to check their predictions through an independent calculation based on an entirely different method.

The photodetachment of $Ga^-$ investigated in the present paper is part of our systematic study of the photodetachment of negative ions from the IIIB group of the periodic system. Negative ions in this group have the $(ns^2\, np^2)\, ^3P$ ground state, and photoexcitation of the $ns$ electron leads to prominent $nsnp^3$ resonances. The accurate description of these resonances is a major challenge for theory. As shown in our recent study of the photodetachment of $B^-$ [10], their interpretation is not trivial and leads to different assignments in different calculations. With the complexity likely increasing in the lower rows of the periodic system, it is interesting to investigate the resonance structure in the entire IIIB group.

The calculations were performed with the $B$-spline $R$-matrix code [11]. The distinctive feature of the approach is the opportunity to employ term-dependent, and hence

*wangkd@htu.cn
†oleg.zatsarinny@drake.edu
‡klaus.bartschat@drake.edu

 

nonorthogonal, sets of one-electron orbitals in the construction of the target states. This allows us to optimize the various atomic wave functions individually, which generally leads to more accurate (compared to multiconfiguration expansions limited to orthogonal orbitals) target descriptions with relatively small configuration expansions. It also provides a systematic way to account for inner-core and core-valence correlations. Furthermore, since we do not impose orthogonality constraints between the continuum functions and the atomic orbitals, we avoid potential inconsistencies between the continuum and the bound parts in the close-coupling expansions. This is very important for an accurate description of resonances, especially when they are located very close to the thresholds and overcorrelation can be a serious issue.

This manuscript is organized as follows. Section II provides an overview of the structure model, followed by a description of the collision calculations needed to describe photodetachment. Results for the latter process, including a detailed analysis of the resonance and threshold structures, is given Sec. III. This is followed by results for the closely related process of elastic scattering from the residual neutral Ga atom in Sec. IV. Unless specified otherwise, atomic units are used.

## II. COMPUTATIONAL DETAILS

The intent of the present paper is to provide a general analysis to clarify the main resonance features and partial-wave contributions. Hence we use a nonrelativistic model, which should be sufficiently accurate, except for energies very close to the fine-structure thresholds.

### A. Target wave functions

In the present calculations the target states of gallium were generated by combining the multiconfiguration Hartree-Fock (MCHF) and the $B$-spline box-based close-coupling methods [12]. The structure of the multichannel target expansion had the form

$$\Phi(4s^2nl, LS) = \sum_{nl} a_{nl}\{\phi(4s^2\,{}^1S)P(nl)\}^{LS} + \sum_{n'l'} b_{n'l'}\{\phi(4s4p\,{}^{1,3}P)P(n'l')\}^{LS} + a\,\varphi(4s\,{}^2\!4p)^2\,P + b\,\varphi(4s4p^2)^{LS}. \quad (1)$$

Here $P(nl)$ denotes the orbital of the outer valence electron, while the $\phi$ and $\varphi$ functions represent CI expansions of the corresponding ionic and specific atomic states, respectively. These expansions were generated in separate MCHF calculations for each state using the MCHF program [13].

The first sum in expansion (1) represents the physical states, whereas the second one represents the core-valence correlation due to the strong $4s$-$4p$ transition. The inner-core (short-range) correlation was introduced by using separate MCHF expansions for the $\phi(4s^2)$ and $\phi(4s4p)$ states. These include all single and double excitations from the $3d$, $4s$, and $4p$ orbitals to the $4l$ and $5l$ ($l = 0$–$4$) correlated orbitals. To keep the final expansions for the atomic states at a reasonable size, all CI expansions were restricted by dropping configurations with coefficients whose magnitude was less than the cutoff parameter of 0.01. The ground state $4s\,{}^2\!4p$ as well as the core-excited states $4s4p^2$ were again included through separate multiconfiguration expansions.

These multiconfiguration expansions ensure the proper inclusion of the short-range correlation in the target wave functions. The core-valence correlation was found to be very important for an accurate representation of the valence orbitals in the $4s^2\,nl$ states, whereas the inner-core correlation was critical to describe the $4s4p^2$ states. Promotion from the $3d$ orbital in the MCHF expansion (i.e., opening up the core) was found to be very important for the correct representation of the relative positions of the $4s^2\,nl$ and $4s4p^2$ subsystems.

The unknown functions $P(nl)$ for the outer valence electron were expanded in a $B$-spline basis, and the corresponding equations were solved subject to the condition that the wave functions vanish at the boundary. The $B$-spline coefficients for the valence orbitals $P(nl)$, along with the various coefficients in Eq. (1), were obtained by diagonalizing the $N$-electron atomic Hamiltonian. The number of spectroscopic bound states that can be generated in the above scheme depends on the $B$-spline box radius. In the present calculations, the latter was set to $50\,a_0$, where $a_0 = 0.529 \times 10^{-10}$ m is the Bohr radius. We employed 104 $B$ splines of order 8 to span this radial range using a semiexponential knot grid. This allowed us to obtain good descriptions of the gallium states with principal quantum number for the valence electron up to $n = 7$.

Table I lists the target states of neutral gallium in the present photodetachment calculations. The calculated binding energies are compared with the available experimental values from the NIST compilation [14]. For the $4s^2\,nl$ states, the agreement between the experimental and theoretical binding energies is satisfactory, with the deviation being less than 40 meV for all bound states, except for the $(4s\,{}^2\!5s)\,{}^2S$ (84 meV) and $(4s4p^2)\,{}^2D$ (141 meV) states. The latter autoionizing state interacts strongly with all $(4s^2\,nd/kd)\,{}^2D$ states and is very

TABLE I. Binding energies (in eV) for gallium target states included in the present CC expansion, compared with the recommended values by NIST [14]. The experimental values were averaged over the fine structure of each multiplet, using a weighting factor proportional to $(2J + 1)$. The NIST values of $-5.9993$ eV and $-5.8969$ eV for the $(4s\,{}^2\!4p)\,{}^2P^o_{1/2,3/2}$ states thus yield an average binding energy of $-5.931$ eV for the ground-state configuration.

| State | Term | NIST [14] | Present | Diff. |
|---|---|---|---|---|
| $4s\,{}^2\!4p$ | ${}^2P^o$ | $-5.931$ | $-5.926$ | 0.005 |
| $4s\,{}^2\!5s$ | ${}^2S$ | $-2.926$ | $-2.842$ | 0.084 |
| $4s\,{}^2\!5p$ | ${}^2P^o$ | $-1.902$ | $-1.852$ | 0.039 |
| $4s4p^2$ | ${}^4P$ | $-1.218$ | $-1.662$ | 0.024 |
| $4s\,{}^2\!4d$ | ${}^2D$ | $-1.687$ | $-1.305$ | 0.034 |
| $4s\,{}^2\!6s$ | ${}^2S$ | $-1.339$ | $-1.198$ | 0.019 |
| $4s\,{}^2\!6p$ | ${}^2P^o$ | $-0.993$ | $-0.973$ | 0.015 |
| $4s\,{}^2\!5d$ | ${}^2D$ | $-0.940$ | $-0.931$ | 0.008 |
| $4s\,{}^2\!4f$ | ${}^2F^o$ | $-0.860$ | $-0.858$ | 0.001 |
| $4s\,{}^2\!7s$ | ${}^2S$ | $-0.772$ | $-0.753$ | 0.019 |
| $4s4p^2$ | ${}^2D$ | 0.671 | 0.530 | $-0.141$ |
| $4s4p^2$ | ${}^2S$ | 1.701 | 1.707 | 0.006 |
| $4s4p^2$ | ${}^2P$ | 2.211 | 2.221 | 0.010 |

difficult to describe. The continuum pseudostates also play a very important role in these expansions. We stress once again that opening the core and considering configurations with excitations out of the $3d$ orbital is crucial to obtain the correct position of the $(4s4p^2)$ states relative the $4s^2\,nl$ subsystem.

### B. Photodetachment calculations

The photodetachment calculations were carried out with the $B$-spline $R$-matrix code [11]. Since the basic theory has been described in detail elsewhere [15], we only give an outline here. In the $R$-matrix approach, the wave function of the $(N+1)$-electron system in the inner region is expanded in terms of energy-independent basis functions

$$\begin{aligned}\Psi_k(x_1,\ldots,x_{N+1}) &= \mathcal{A}\sum_{ij}\bar{\Phi}_i(x_1,\ldots,x_N;\hat{\mathbf{r}}_{N+1}\sigma_{N+1})\,r_{N+1}^{-1}\,B_j(r_{N+1})\,a_{ijk} \\ &\quad+\sum_i \chi_i(x_1,\ldots,x_{N+1})\,b_{ik}. \end{aligned} \tag{2}$$

Here the $\bar{\Phi}_i$ denote the channel functions constructed from the $N$-electron target states, while the splines $B_j(r)$ represent the continuum orbitals. The $\chi_i$ are additional $(N+1)$-electron bound states. In standard $R$-matrix calculations [16], the latter are included one configuration at a time to ensure completeness of the total trial wave function and to compensate for orthogonality constraints imposed on the continuum orbitals. The use of nonorthogonal one-electron radial functions in the BSR method, on the other hand, allows us to avoid these configurations solely for compensating orthogonality restrictions.

Nevertheless, bound channels were employed in the present BSR calculations for a more accurate description of the $4s^{\,2}4p^2$ and $4s4p^3$ states of $Ga^-$. For these states we also used separate multiconfiguration expansions with single and double promotions out of the $3d$, $4s$, and $4p$ subshells. An important issue concerns the choice of the cutoff parameters in these expansions. Note that the convergence for the negative-ion states is much slower than for the neutral atom. By choosing the cutoff parameter as 0.004, we obtained an electron affinity of 0.429 eV, which is very close to the experimental value of 0.430 eV [6]. The same cutoff parameter was then used for all other $4s^{\,2}4p^2$ and $4s4p^3$ states of $Ga^-$.

The scattering model in the present calculations contains all target states generated by the expansion (1) up to the highest $4s4p^2$ target state with term $^2P$; see Table I. It couples the 13 physical target states shown in the table, plus seven bound pseudostates $4s^2\,nl$ below and another 12 continuum pseudostates $4s^2\,nl$ above the ionization threshold. This model is expected to fully describe photodetachment from both the $4p$ and $4s$ subshells. Overall, the close-coupling equations contains 32 target states, which result in up to 73 scattering channels (for the $^3P$ partial wave). This model will be labeled as BSR-32 below.

In $R$-matrix theory, the photodetachment cross section is defined through the dipole matrix elements between the initial state $\Psi_0$ and the $R$-matrix basis states $\Psi_k$, provided that all radial orbitals of the initial state are well confined to the inner region. The total photodetachment cross section (in $a_0^2$) for a photon energy $\omega$ (in Rydbergs) and an initial state with total orbital angular momentum $L_0$ is given by

$$\sigma(\omega) = \frac{4}{3}\pi^2\alpha\frac{\omega C}{(2L_0+1)}\sum_j |(\Psi_j^-\|D\|\Psi_0)|^2, \tag{3}$$

where $\alpha\approx 1/137$ is the fine-structure constant and $D$ is the electric dipole operator. It could be either in the length or the velocity form, with $C=1$ in the former and $C=4/\omega^2$ in the latter case. The index $j$ runs over the various open channels.

Expanding the $\Psi_j^-$ in terms of the $R$-matrix states, we find that

$$(\Psi_j^-\|D\|\Psi_0) = \frac{1}{a}\sum_k \frac{(\Psi_k\|D\|\Psi_0)}{E_k-E_0-\omega}\boldsymbol{w}_k^T\boldsymbol{R}^{-1}\boldsymbol{F}_j^-(a), \tag{4}$$

where $(\Psi_k\|D\|\Psi_0)$ are reduced matrix elements between the initial state and the $R$-matrix basis functions, $\boldsymbol{w}_k^T$ stands for the surface amplitudes of the inner-region solutions at $r=a$, and $\boldsymbol{R}^{-1}$ is the inverse of the $R$-matrix [11]. The energies $E_k$ and $E_0$ are also in Rydbergs. If all channels are open (for details regarding the modifications necessary if some channels are closed, see Ref. [16]), the asymptotic form of the radial wave functions $F_i(r)$ for the scattered electron may be expressed in the form

$$\boldsymbol{F}(r)\sim \boldsymbol{k}^{-1/2}(\boldsymbol{S}+\boldsymbol{C}\boldsymbol{K}). \tag{5}$$

Here we have written the channel momenta, $\boldsymbol{k}$, as a diagonal matrix. The diagonal matrices $\boldsymbol{S}$ and $\boldsymbol{C}$ correspond to regular and irregular Coulomb (or Riccati-Bessel) functions in each scattering channel. The asymptotic expression (5) defines the reactance $K$ matrix, $\boldsymbol{K}$, which is appropriate for standing-wave boundary conditions. For photodetachment, on the other hand, the solutions $\Psi_j^-$ correspond to asymptotic conditions with a plane wave in the direction of the ejected electron momentum $\boldsymbol{k}$ and ingoing waves in all open channels. The corresponding radial functions $\boldsymbol{F}^-$ are related to the $\boldsymbol{F}$ with the $K$-matrix asymptotic form via

$$\boldsymbol{F}^- = -i\boldsymbol{F}(1-i\boldsymbol{K})^{-1}. \tag{6}$$

The program ASYPCK [17] was used to generate the asymptotic solutions $\boldsymbol{F}$.

## III. RESULTS FOR PHOTODETACHMENT

Figure 1 exhibits our results for the total photodetachment cross section of $Ga^-(4s^{\,2}4p^2)\,^3P$ in the photon energy range from threshold to 12 eV. As seen from the figure, our length-form and velocity-form predictions agree very well with each other at all energies, with the difference not exceeding 20%. While not a proof, this is a strong indicator regarding the overall high quality of the wave functions used in the calculations. The remaining differences are due to restrictions imposed on the target expansions. The energy dependence of the photodetachment cross section exhibits noticeable structure, with several maxima and minima, both narrow and wide. Below we will classify most of these features, as possible negative-ion resonances or related to opening of channels at various thresholds. This will be done by thoroughly analyzing the partial-wave cross sections and the contributions from dominant individual ionization channels.

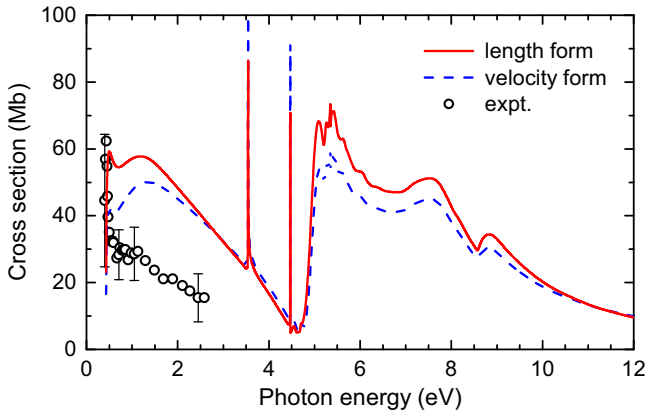


FIG. 1. Total photodetachment cross sections of $Ga^-$ obtained with the length (solid line) and velocity (dashed line) forms of the electric dipole operator. Our results are compared with the experimental data of Feldmann *et al.* [8] (open circles) that are shown with a few representative error bars.

### A. $^3P$ photodetachment

To our knowledge, no other theoretical results are available for comparison. The only published work that we are aware of are the data of Feldmann *et al.* [8]. They used a crossed-beam apparatus with a conventional light source for photoelectron energies between 0.5–2.6 eV. As seen from Fig. 1, our results are considerably larger than the measured cross sections in this energy region. Note, however, that the experimental error bars in the figure only represent the statistical uncertainty. The uncertainty in the absolute normalization was estimated to within 50%. We also note that the absolute cross sections from the measurements by Feldmann *et al.* [8] for other ions differ considerably from currently available data from other experiments. For example, comparison for the photodetachment of $B^-$ [10] showed that the absolute cross sections published in Ref. [8] are smaller by about a factor of two than other experimental data and theoretical predictions. This suggests that their absolute normalization could be problematic. Additional measurements would be highly desirable to shed more light on, and hopefully resolve, these discrepancies.

In order to properly resolve the possible resonance structures, we used small steps of $10^{-4}$ Ry when varying the incident photon energy in our calculations. Resonances correspond to the temporary trapping of an electron to form a short-lived quasibound state, and they are key features in understanding many electron-atom scattering processes at low energies. In the vicinity of a resonance, the cross section often changes sharply with energy, and the eigenphase sum changes by a factor of about $\pi$ radians over a relatively narrow energy range. By analyzing the eigenphase sums calculated within the present model, we obtained the resonance parameters (position and width) listed in Table II along with their tentative assignments. For their further discussion, it is most convenient to investigate each partial wave separately.

According to the dipole selection rules, the photodetachment of the ground state of $Ga^-(4s^2 4p^2\, ^3P)$ will result in three final continuum states with total symmetries $^3D^o$, $^3P^o$, or $^3S^o$, respectively. Figure 2 shows the partial cross section for the $^3P^e \rightarrow {}^3D^o$ transition and the corresponding dominant channels. The first broad peak in the partial cross section comes from the $4s^2 4p(^2P^o)kd$ scattering channel, which is the dominant channel for this partial wave. The cross section for this channel is strongly affected by the wide $Ga^-(4s4p^3\, ^3D^o)$ resonance at 4.959 eV. This highly asymmetric Fano resonance, with a window feature at 4.619 eV and a peak at 5.095 eV, is the principal feature in the $Ga^-$ photodetachment. It is similar to the feature seen in the more frequently studied photodetachment of $B^-$ [10]. We also detected an additional narrow resonance, classified as

TABLE II. Parameters of identified $Ga^-$ resonances (in eV).

| Classification | Photon energy | Width |
|---|---|---|
| $4s^2 5s5p\, ^3P^o$ | 3.543 | 0.006 |
| $4s^2 5p6s\, ^3P^o$ | 4.468 | 0.002 |
| $4s4p^3\, ^3D^o$ | 4.959 | 1.534 |
| $4s4p^3\, ^3P^o$ | 5.259 | 0.306 |
| $4s^2 5d6p\, ^3D^o$ | 5.351 | 0.010 |
| $4s4p^3\, ^1D^o$ | 7.052 | 0.752 |
| $4s4p^3\, ^1P^o$ | 7.461 | 0.312 |
| $4s4p^3\, ^3S^o$ | 7.940 | 1.674 |

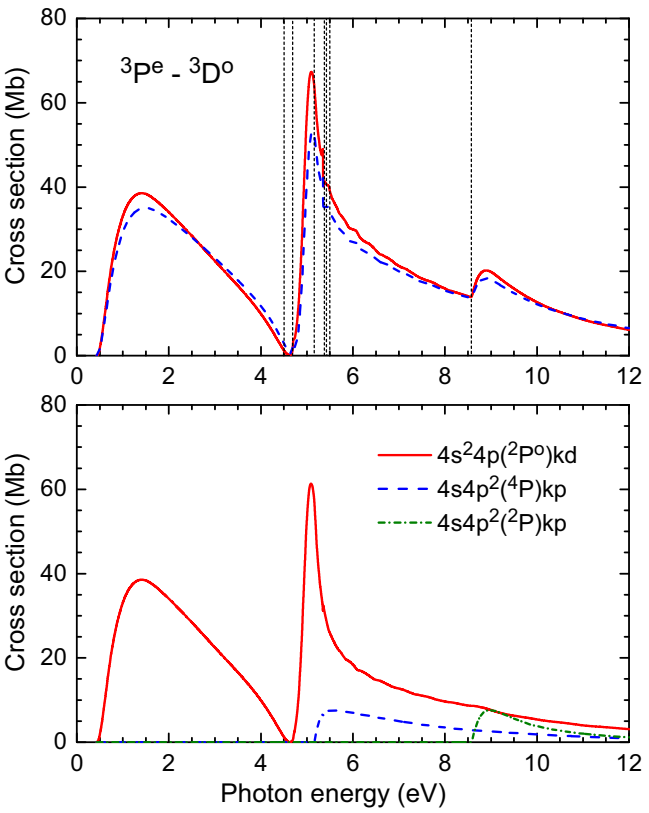


FIG. 2. Top: Partial cross section for the $^3P^e$-$^3D^o$ transition obtained in the length (solid line) and velocity (dashed line) forms of the electric dipole operator. The vertical lines represent the target thresholds. Bottom: Main contributions (as obtained in the length form) from individual scattering channels for the $^3D^o$ partial cross section.

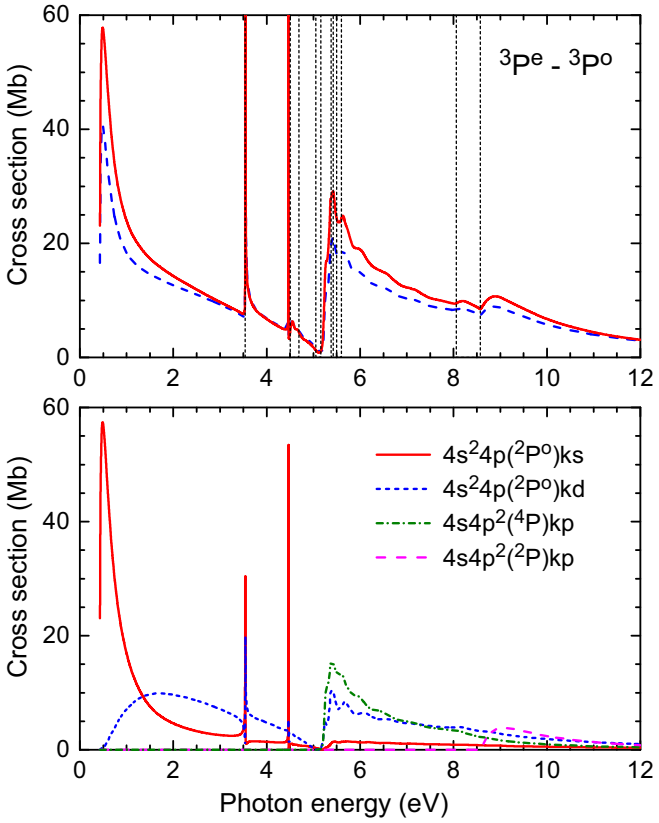


FIG. 3. Top: Partial cross section for the $^3P^e$-$^3P^o$ transition obtained in the length (solid line) and velocity (dashed line) forms of the electric dipole operator. The vertical lines represent the target thresholds. Bottom: Main contributions (as obtained in the length form) from individual scattering channels for the $^3P^o$ partial cross section.

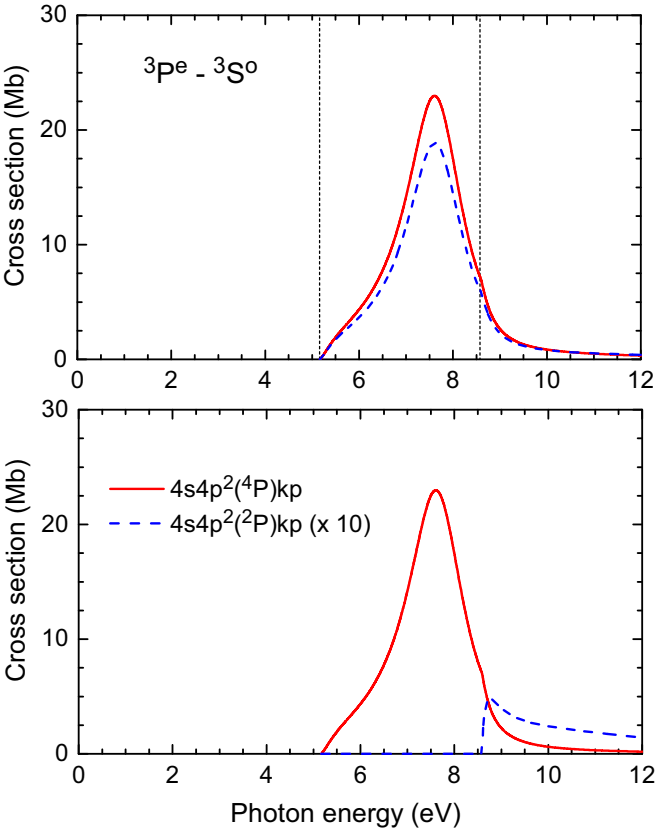


FIG. 4. Top: Partial cross section for the $^3S^e$-$^3P^o$ transition obtained in the length (solid line) and velocity (dashed line) forms of the electric dipole operator. The vertical lines represent the target thresholds. Bottom: Main contributions (as obtained in the length form) from individual scattering channels for the $^3S^o$ partial cross section.

$4s^2 5d6p\,^3D^o$, at 5.351 eV. The broad maximum at 8.85 eV is due to the opening of the $4s4p^2(^2P)kp$ channel. In general we found that direct photodetachment through the $4s$-$kp$ and $4p$-$kd$ transitions represents the dominant processes. All other scattering channels provide only very small contributions.

In Fig. 3, we show the cross section resulting in the $^3P^o$ final symmetry. The steep rise near threshold originates from the $4s^2 4p(^2P^o)ks$ channel, which exhibits the characteristics of $s$-wave scattering. With increasing photon energy, the $4s^2 4p(^2P^o)kd$ channel gains intensity and becomes dominant. The first sharp resonant peak, located at 3.543 eV, is identified as the $4s^2 5s5p\,^3P^o$ Fano-type resonance. This resonance appears in all energy-allowed channels, as indicated by its decay into all open channels. The second sharp peak at 4.468 eV, just below the $4s^2 5p$ target state, is associated with the $4s^2 5p6s^3P^o$ resonance. The wide structure with a window at 5.150 eV and a subsequent peak is due to another asymmetric Fano resonance of principal configuration $(4s4p^3\,^3P^o)$. Its parameters are given in Table II. The left wing of this resonance is strongly disturbed by many other opening channels, thereby leading to additional small structures. The two maxima at higher energies are associated with the $4s4p^2(^2S)kp$ and $4s4p^2(^2P)kp$ channels during the $4s$ photodetachment. Subsequent autoionization of these $4s4p^2$ states leads to double photodetachment and ultimately $Ga^+$.

Figure 4 shows the partial cross sections for the $^3S^o$ symmetry. This partial wave involves only two target states, $Ga(4s4p^2)\,^4P$ and $Ga(4s4p^2)\,^2P$, and the cross sections are dominated by a strong wide peak at 7.940 eV. We classify this feature as the $Ga^-(4s4p^3)\,^3S^o$ resonance. It lies between its parent states with principal configuration $4s4p^2$ and hence cannot be considered a regular Feshbach resonance. In neutral atoms or positive ions, Feshbach resonances can often be represented by the parent state plus a captured electron. For negative-ion quasibound states, however, such a physical picture does not work since, due to the weak Coulomb nuclear attraction, the captured electron may affect the orbitals in the parent state considerably, especially in the case of equivalent electrons. In our case, for example, the mean radius of the $4p$ electron changes from $3.13\,a_0$ in the $Ga(4s4p^2)$ parent states to $4.30\,a_0$ in the $Ga^-(4s4p^3)$ states. This leads to a considerable change in the electron-electron interaction strength between the valence electrons, which in turn may push up the energy of the resulting negative-ion quasibound state. As another consequence, such kind of resonances cannot be well described in a pure close-coupling expansion with fixed target wave functions.

Analyzing the channel cross sections represented in Figs. 2–4 allows us to draw conclusions about the

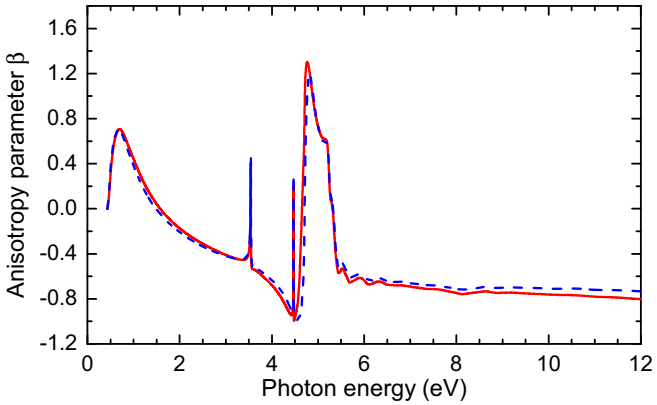


FIG. 5. BSR-13 anisotropy parameter $\beta$ in the photon energy range from threshold to 12 eV obtained in the length (solid line) and velocity (dashed line) forms of the electric dipole operator.

photodetachment to the individual residual target states. As expected, the main contributions originate from the detachment of a $4p$ electron, thus leaving the target in its ground state $\mathrm{Ga}(4s^2 4p)^2 P^o$, and from $4s$ detachment leaving the target in the excited $\mathrm{Ga}(4s4p^2)\,^4P^o$ and $(4s4p^2)\,^2P^o$ states. The $4s$ photodetachment even becomes dominant in the vicinity of the $\mathrm{Ga}^-(4s4p^3)\,^3S^o$ resonance. All other channels yield almost negligible contributions, while nevertheless leading to small additional structures.

Along with total photodetachment cross sections, photoelectron angular distributions (PADs) are important in structural studies of atoms and ions. The asymmetry parameter $\beta$ completely characterizes the shape of the PAD pattern. Investigation of the asymmetry parameter near autodetaching resonances can reveal the role of correlation effects or relativistic interactions in the process. The asymmetry parameter for the $\mathrm{Ga}^-$ photodetachment process from threshold to 12 eV is depicted in Fig. 5. Our results clearly indicate the complicated energy dependence of this parameter. Several sharp peaks, as well as the broad peak around 4.7 eV, are due to the corresponding resonances.

### B. $^1D$ photodetachment

According to our calculations, the $\mathrm{Ga}^-$ ion has an excited $(4s^2 4p^2)\,^1D^e$ bound state with a binding energy of 0.097 eV. This state may thus contribute to the total photodetachment of $\mathrm{Ga}^-$, and the corresponding cross sections would be needed for the interpretation of any experimental measurements. The total and partial photodetachment cross sections for the $^1D^e$ initial state are presented in Fig. 6. Compared to the results for the $^3P^e$ ground state, the cross sections are larger and again exhibit prominent resonance-like structures. Not all peaks, however, can be related to particular resonances. The eigenphase analysis shows that only two peaks (at 7.052 eV for the $^1D^o$ partial wave and at 7.461 eV for the $^1P^o$ partial wave) are due to the corresponding $4s4p^3$ negative-ion states (see Table II). All other structures reflect near-threshold maxima caused by the opening of new channels. Most noticeable are the near-threshold maxima in the $4s^2 4pks$, $4s^2 5skp$, and $4s4p^2(^2P)kp$ channels for the $^1P^o$ partial wave, the $4s4p^2(^2P)kp$ channel for the $^1D^o$ partial wave, and the

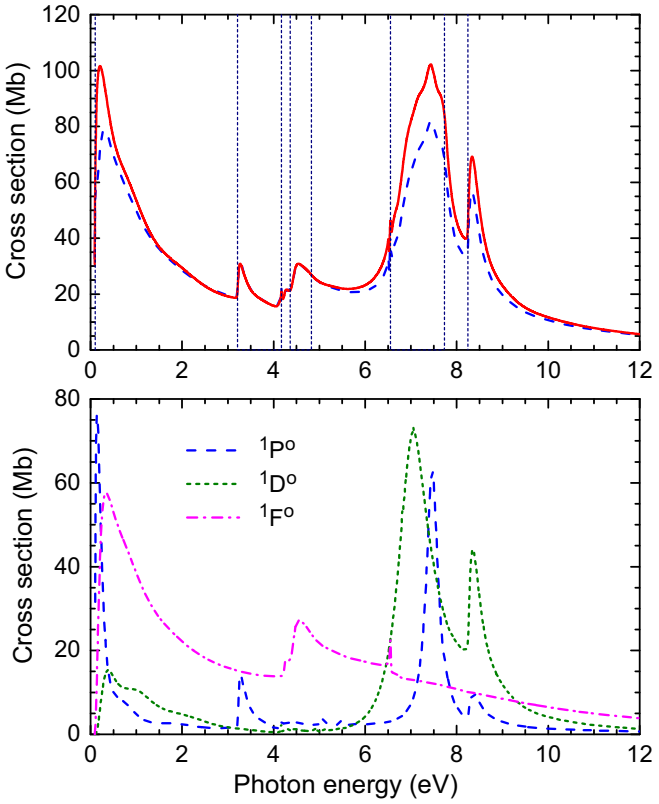


FIG. 6. The total (top) and the most important partial (bottom) photodetachment cross sections of $\mathrm{Ga}^-$ from the $^1D^e$ state. The latter were obtained in the length form of the electric dipole operator.

$4s^2 4pkd$ and $4s^2 4dkp$ channels for the $^1F^o$ partial wave. Note that many peaks are located above the ionization limit of Ga at 5.999 eV (relative to the ground state of Ga) and are associated with the $4s4p^2$ final target states. Subsequent autoionization of these states will result in double photodetachment, leading to the $\mathrm{Ga}^+$ positive ion as the final product of the reaction.

## IV. ELASTIC SCATTERING

Elastic scattering at low energies is closely related to the photodetachment process, since the partial waves for the photodetached electron (and more, due to the lack of dipole selection rules) also appear in the description of the scattering process. The elastic cross section shown in Fig. 7 exhibits a complex energy dependence due to various partial-wave and resonance contributions. The dominant partial-wave contributions are also shown. In particular, the shoulder at 0.1 eV is due to the $(4s^2 4p^2)\,^1S^e$ resonance. At higher energies, the main contribution comes from a $p$-wave scattered electron in the $(4s^2 4pkp)\,^1D^e$ and $^3P^e$ partial waves. Near the first excitation thresholds around 3 eV and for another few eV above those, there is noticeable resonance structure. Narrow features appear due to the $4s^2 nln'l'$ doubly-excited states, whereas the wider structure is mainly due to the $4s$-excited $4s4p^3$ states, as discussed previously in the photodetachment cross sections.

The elastic cross section at threshold is finite, and it is mainly determined by the $(4s^2 4pks)\,^3P^o$ channel. We predict

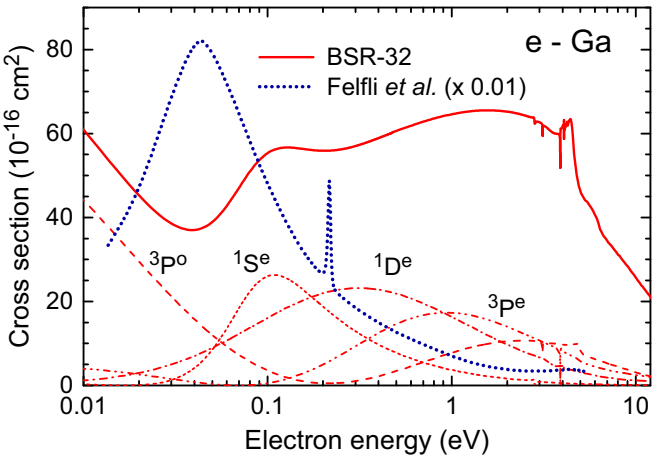


FIG. 7. Angle-integrated elastic cross section for electron scattering from atomic Ga in its ground state. In addition to the present BSR-32 and the dominant partial-wave contributions, we also show the predictions of Felfli *et al.* [9]. Note the entirely different energy dependence of the latter results and the fact that they were multiplied by a factor of 0.01.

a scattering length of $-4.8\,a_0$. This partial wave also exhibits a Ramsauer minimum at 0.2 eV. The scattering length for the $(4s^2 4pks)\,^1P^o$ channel comes out as $-1.3\,a_0$ in our model, hence giving a much smaller contribution to the cross section at low energies than the $^3P^o$ channel.

The somewhat significant contributions from partial waves other than $^3P^o$ and $^1P^o$ (e.g., $^3P^e$) at the lowest energy of 0.01 eV, for which we performed calculations, suggests the possible importance of higher-multipole (mostly quadrupolar) interactions. We refrain from further speculations, however, because (i) calculations at even lower energy should be performed to be sure, and (ii) such calculations in a nonrelativistic framework would likely not be meaningful, since the fine-structure splitting of the Ga ground state (0.102 eV [14]) should be accounted for at such low energies.

The accurate description of elastic scattering in this low-energy regime requires a very good representation of the target polarization due to the scattering electron. The BSR-32 expansion yields a ground-state polarizability of $48.8\,a_0^3$, in good agreement with other available calculations [18] that yield values in the range from 49 to $55\,a_0^3$. This suggests that contributions from coupling to higher-lying target continuum states omitted in the present model are relatively small and do not exceed 10 %.

The only available comparison with our results involves the total cross section for the e-Ga collision problem calculated by Felfli *et al.* [9], who used a complex angular-momentum approach. The total cross section up to the first excitation threshold at 3.073 eV is completely comprised of elastic scattering. As seen in the figure, our predictions for the elastic cross sections differ dramatically from those of Felfli *et al.* [9], regarding both the magnitude and the energy dependence. The differences amount to more than two orders of magnitude at low energies.

Felfli *et al.* interpreted their results as a strong shape resonance, but no additional details concerning, for example, the angular momentum for the scattered electron in this resonance, were provided. The narrow peak at 0.222 eV was interpreted as a resonance due to the ground state of $Ga^-$, presumably of the $(4s^2 4p^2)\,^3P$ configuration. Given that this state is well known to be bound and that our results for the photodetachment cross section only differ by a factor of two from experiment (a deviation that can be explained to some extent), a further discussion of the differences between our results and those of Felfli *et al.* does not seem warranted. Nevertheless, we presented their results for completeness.

## V. SUMMARY

We performed a detailed study of the photodetachment of $Ga^-$ and presented results for the total as well as partial cross sections for the principal scattering channels. We analyzed the resonance structure and also showed the asymmetry parameter for the photoelectron angular distribution. The calculations were performed with the *B*-spline *R*-matrix method, where the use of nonorthogonal orbital sets allows for high flexibility, and hence accuracy, in the construction of the target wave functions. The possibility of individually optimizing the one-electron orbitals for each state of interest is very important for this problem, especially since we found considerable orbital relaxation during the photodetachment process. Our results, obtained in the length and the velocity forms of the electric dipole operator, agree very well with each other.

The energy dependence of the photodetachment cross section exhibits several distinctive features. To clarify the threshold and resonance structure, both the partial cross sections and the principal contributions of individual ionization channels to the partial cross sections were analyzed in detail. Studying such prominent features provides opportunities for future investigations of the $Ga^-$ negative ion. In light of the deviations (by about a factor of two in magnitude) between our predictions and the only currently available absolute measurements, additional experiments and calculations are desirable to hopefully resolve the discrepancy.

An enormous discrepancy (two orders of magnitude) with the only other published theoretical results for electron collisions with neutral Ga was found for the elastic cross sections. We have no definite explanation for this discrepancy, but we do believe that the present calculations are reliable.

Finally, we emphasize that the current calculations were performed in a nonrelativistic framework, in order to get a feeling for the complexity of the problem. If sufficiently accurate experimental data or results from other calculations that included relativistic effects were to become available, it would be appropriate (and feasible) to extend the present model as well.

## ACKNOWLEDGMENTS

This work was supported by the United States National Science Foundation under Grants No. PHY-1212450, No. PHY-1403245, and No. PHY-1520970. K.W. was supported by the Joint Fund for Fostering Talents of the National Natural Science Foundation of China and Henan Province under Grant No. U1504109. He would like to thank Drake University for the hospitality during his visit.

[1] H. Massey, *Negative Ions* (Cambridge University Press, Cambridge, 1976).
[2] S. J. Adelman, C. R. Proffitt, G. M. Wahlgren, D. S. Leckrone, and L. Dolk, Astrophys. J. Suppl. Ser. **155**, 179 (2004).
[3] F. Arnau, F. Mota, and J. J. Novoa, Chem. Phys. **166**, 77 (1992).
[4] W. P. Wijesundera, Phys. Rev. A **55**, 1785 (1997).
[5] E. Eliav, Y. Ishikawa, P. Pyykkö, and U. Kaldor, Phys. Rev. A. **56**, 4532 (1997).
[6] W. W. Williams, D. L. Carpenter, A. M. Covington, M. C. Koepnick, D. Calabrese, and J. S. Thompson, J. Phys. B: At. Mol. Opt. Phys. **31**, L341 (1998).
[7] D. Sundholm, M. T. Tokman, P. Pyykkö, E. Eliav, and U. Kaldor, J. Phys. B: At. Mol. Opt. Phys. **32**, 5853 (1999).
[8] D. Feldmann, R. Rackwitz, E. Heinicke, and H. J. Kaiser, Z. Naturf. A **32a**, 302 (1977).
[9] Z. Felfli, A. Z. Msezane, and D. Sokolovski, J. Phys. B: At. Mol. Opt. Phys. **45**, 045201 (2012).
[10] K. Wang, O. Zatsarinny, and K. Bartschat, Eur. Phys. J. D **70**, 72 (2016).
[11] O. Zatsarinny, Comput. Phys. Commun. **174**, 273 (2006).
[12] O. Zatsarinny and C. F. Fischer, Comput. Phys. Commun. **180**, 2041 (2009).
[13] C. F. Fischer, Comput. Phys. Commun. **176**, 559 (2007).
[14] http://physics.nist.gov/cgi-bin/AtData
[15] O. Zatsarinny and C. F. Fischer, J. Phys. B: At. Mol. Opt. Phys. **33**, 313 (2000).
[16] P. G. Burke, *R-Matrix Theory of Atomic Collisions: Application to Atomic, Molecular and Optical Processes* (Springer, New York, 2011).
[17] M. A. Crees, Comput. Phys. Commun. **19**, 103 (1980).
[18] http://ctcp.massey.ac.nz/dipole-polarizabilities